Tribol Lett (2015) 60:34
DOI 10.1007/s11249-015-0610-6

ORIGINAL PAPER

Pressure–Viscosity Coefficient of Hydrocarbon Base Oil through Molecular Dynamics Simulations

Pinzhi Liu[1] · Hualong Yu[1] · Ning Ren[2] · Frances E. Lockwood[2] · Q. Jane Wang[1]

Received: 31 July 2014 / Accepted: 8 October 2015 / Published online: 30 October 2015

Abstract The pressure–viscosity coefficient (the α value), which represents the variation of viscosity as a function of pressure, is an important parameter for elastohydrodynamic lubrication analyses. The properties of hydrocarbons in the C_{20}–C_{40} mass range are of fundamental importance as they are basic constituents of synthetic- and mineral-based lubricant stocks. The conventional acquisition of the α value requires preparation of lubricant samples and experimental testing by means of a high-pressure viscometer. In this paper, we present a method to obtain the α value of a typical base oil (1-Decene trimer) based solely on the molecular dynamics simulations. Non-equilibrium molecular dynamics (NEMD) simulations were performed to calculate the shear viscosity of the lubricant at various temperatures and pressures up to 1 GPa. Elevated temperatures and time–temperature superposition (TTS)-based extrapolations were applied to further extend the ability of the NEMD simulations, and the rotational relaxation time was calculated and used to determine the validity of the NEMD calculations. The α value at 100 °C was calculated and compared with experimental results. Effectiveness of the extrapolation was evaluated with a 95 % confidence interval.

Keywords Pressure–viscosity coefficient · Molecular dynamics simulations · Base oil · Hydrocarbon

✉ Q. Jane Wang
qwang@northwestern.edu

[1] Center for Surface Engineering and Tribology, Northwestern University, 2145 Sheridan Road, Evanston, IL 60208, USA

[2] Ashland Inc., Lexington, KY, USA

1 Introduction

Rheological properties of a lubricant are determined by the molecular structures of its base oil and additives. The properties of alkane in the C_{20}–C_{40} mass range are of fundamental importance because they are key constituents of the base stocks of synthetic and mineral lubricants. In elastohydrodynamic lubrication (EHL), the pressure–viscosity coefficient, α, which has been used to characterize the pressure dependence of the shear viscosity, is critical for evaluating the lubricant film thickness at the contact interface under a high pressure in the mega- and giga-pascal ranges, where the viscosity properties change significantly from those at the ambient conditions. Therefore, an accurate evaluation of the shear viscosity at such a high pressure is of great importance.

The most commonly used definition of α comes from the exponential viscosity–pressure relationship [1], shown below,

$$\eta(T,P) = \eta(T,0)e^{\alpha(T)P} \tag{1}$$

where $\eta(T, P)$ is the viscosity at pressures P and temperatures T.$\eta(T, 0)$ represents the viscosity value at the atmospheric pressure and temperature T. In practice, the ambient pressure–viscosity coefficient,

$$\alpha_0 = \frac{1}{\eta}\frac{\partial\eta}{\partial P}\bigg|_{P=0} \tag{1a}$$

and the reciprocal asymptotic isoviscous pressure, which is a generalized pressure–viscosity coefficient,

$$\alpha^* = \left[\int_0^\infty \frac{\eta_0 dP}{\eta(P)}\right]^{-1} \tag{1b}$$

are often used with a piecewise integration from test data points [2].

The Walther equation has been widely used to characterize the viscosity relationship with temperature [3, 4], and is the basis for the ASTM viscosity–temperature charts, shown below,

$$\log\log(v + c) = a - b\log T, \tag{2}$$

where v is the kinematic viscosity, T is the temperature in Kelvin, a and b are lubricant-specific parameters and c is a constant, which is about 0.7. The Vogel–Fulcher–Tammann–Hesse (VFTH) equation [5–7], shown below,

$$\log_e(\eta) = A + \frac{B}{T - T_0} \tag{3}$$

was also used over a wide viscosity range for many liquids, and is considered more accurate [8]. However, its nonlinear nature and three fluid specific coefficients make it more difficult for generalization [3].

Currently, most α-value evaluations have been performed by means of testing. Viscometers and rheogoniometers are often seen for viscosity measurements at atmospheric conditions. Developments of new viscometers have allowed valuable high-pressure viscosity measurements at 1 GPa or higher [9–11]. EHL film measurements combined with the Hamrock–Dowson equation [12, 13] have also been utilized to determine the pressure–viscosity coefficient. α-Value acquisitions have also been performed using empirical correlations with other related material properties [14, 15].

However, preparations and measurements of lubricant samples can be expensive to perform and difficult to do, especially for viscosity measurements at a high pressure and large shear rate. Moreover, lubricant samples, even "pure" base oils, are often mixtures of several different molecular chains, for which the measured results are generally resultant responses from all major constituents. The effect and influence of each component on the lubricant properties can hardly be determined simply through testing.

The implementation of molecular dynamics simulations for the viscosity evaluation of alkanes has gained momentum since the 1990s, benefited by the increase in computational power and development of advanced numerical models [16–20]. Equilibrium molecular dynamics (EMD) and non-equilibrium molecular dynamics (NEMD) [21] simulations are widely used for this purpose. NEMD simulations of steady shear flow, in particular, can lead directly to the shear viscosity calculation.

Rheological properties of a wide range of alkanes have been studied through molecular dynamic simulations, with the strain-rate-dependent viscosities a major focus of the studies. Morriss et al. [22] examined the rheology of *n*-decane and *n*-eicosane; Cui et al. [23, 24] showed NEMD results for *n*-decane, *n*-hexadecane, *n*-tetracosane, 10-*n*-hexylnonadecane and squalane; and Khare et al. [25] studied *n*-docosane, *n*-octacosane and 5,12-dipropylhexadecane. In these studies, a Newtonian plateau has been observed at low shear rates; and at high shear rates, alkanes demonstrate a shear thinning behavior over several magnitudes of strain rate. The influence of branches of isomers on their viscosity values has also been of interest. Kioupis and Maginn [26] compared the rheological properties of three isomers of C_{18}. Moore et al. [27] examined the rheological behavior of isomers of C_{30} and reached the C_{20}–C_{40} range for base oils. Both studies showed that long, widely spaced branches should have better temperature performances than those with short, closely packed branches. Jabbarzadeh et al. [28] studied the rheological properties of a number of molecular shapes of C_{100}. Though the calculations were only in the non-Newtonian domain due to the limitation of NEMD, they further demonstrated that the effective length of the molecule and its degree of branching ultimately dictate its shear response. Attempts to used MD simulations to acquire temperature–viscosity and pressure–viscosity coefficients have also been reported. Predictions of viscosity index (VI) or viscosity number (VN) of squalane [29], *n*-octadecane [26] and 9-octyldocosane [27] have all been reported. Pressure–viscosity coefficients have been calculated through EMD [30] and NEMD [31, 32], with the latter approach more successful than the former. Results for viscosity dependence on pressure and temperature have shown that while the applied MD models underpredict the actual Newtonian viscosity, they can determine the temperature or pressure dependence of viscosity with a reasonable accuracy.

However, a major challenge for applying the MD simulation to viscosity evaluation other than the inaccuracy at the Newtonian regime due to the effectiveness of the force field is the low signal-to-noise ratio that could result in an impractically high shear rate, and the catch of only the non-Newtonian regime of the shear-rate dependent viscosity. In NEMD simulations, the minimum achievable shear rate is usually around $10^8\ s^{-1}$ at the ambient temperature and pressure due to the low signal-to-noise ratio [23], and this shear rate is higher than that appear in most current engineering applications. More importantly, a lubricant may experience temporary shear thinning, in which the shear stress induces molecular alignment and lowers the effective viscosity [33]. Figure 1 shows the change of shear viscosity with increasing shear rate for a typical lubricant. In the low shear-rate region, the shear stress in the fluid increases linearly with shear rate, showing the first Newtonian plateau. The transition from Newtonian to non-Newtonian regime takes place at the critical shear rate $\dot{\gamma}_{cr}$, corresponding to the onset of the shear thinning behavior. As shear rate further increases, effective viscosity decreases until sometimes the second Newtonian plateau is reached. In order to capture the first Newtonian plateau, the

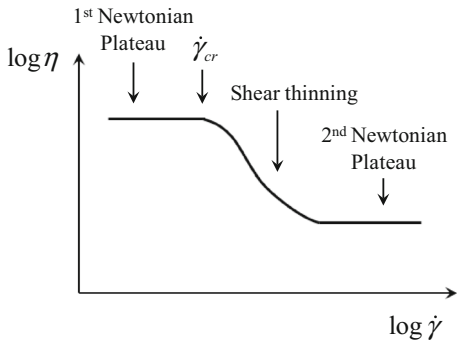

Fig. 1 Typical change of shear viscosity with increasing shear rate

shear rate applied in the NEMD simulations must be smaller than the critical shear rate. For alkane fluids, studies have shown that the critical shear rate is about the reciprocal of the rotational relaxation time [24]. For molecules of a larger carbon number or for lubricants at low temperatures and/or high pressure, the systems show "slow" dynamics or long relaxation times [34], making it even more difficult to calculate the first Newtonian plateau at high pressures.

Many efforts have been committed to overcome this difficulty. Gordon attempted to predict viscosity of heavier molecules based on the Stokes–Einstein relationship [35]. Pan and McCabe [36] applied the transient time correlation function (TTCF) formalism [37, 38] to calculate the viscosity of *n*-decane. Their results showed that the TTCF method agreed well with NEMD for viscosity calculations, and the shear rate was able to reach as low as 10^4 s^{-1}. Bair et al. [39] applied the concept of time–temperature superposition (TTS) successfully and compared the NEMD simulation results with experimental viscosity data for squalane. A master curve for shear-rate dependent viscosity was acquired based on the experimental and MD results because it was difficult to calculate the low-shear viscosities at the ambient temperature and high pressure directly from MD.

1-Decene trimer is a major component of poly-α-olefin (PAO) 4 cSt, or PAO 4, an important fluid in the current synthetic base oil market. Its molecular structure, shown in Fig. 2, may also be considered as a representative structure

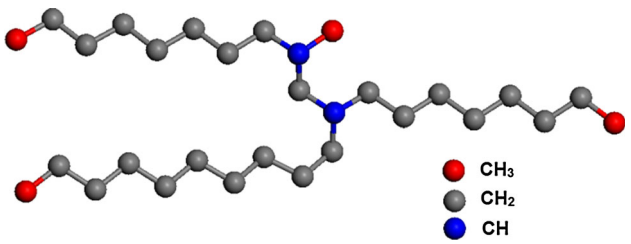

Fig. 2 Molecular structure of 1-Decene trimer

for all branched alkanes in the C_{20}–C_{40} range. Understanding the lubrication properties of the 1-Decene trimer requires the knowledge of its pressure–viscosity coefficient. The research reported in this paper is aimed at acquiring the α value of the 1-Decene trimer based solely on MD calculations using the concept of TTS.

2 Model Description

Acquisition of the pressure–viscosity coefficient for 1-Decene trimer requires the shear viscosity values in a range of pressures and the assurance that the first Newtonian plateau can be successfully captured through NEMD simulations, i.e., the applied NEMD shear rate is lower than the critical shear rate. To achieve such assurance, the applicable NEMD shear rate is compared with the reciprocal of the rotational relaxation time. The latter is calculated through the integration of the reorientation autocorrelation function [40], shown below,

$$\tau = \int_0^\infty C^1(t)\mathrm{d}t = \int_0^\infty \left\langle \left(\overrightarrow{e_1(t)} \cdot \overrightarrow{e_1(0)}\right)\right\rangle \mathrm{d}t, \tag{4}$$

where $C^1(t)$ is the reorientation autocorrelation function. For branched hydrocarbons, $\overrightarrow{e_1(t)}$ and $\overrightarrow{e_1(0)}$ are unit vectors representing the longest principal axis of the molecule ellipsoid of inertia at time interval t and initial point, respectively. The principle axes were determined from the eigenvectors of the symmetric inertia tensors of the molecule.

The modified Kohlrausch–Williams–Watts (mKWW) function [41], shown below, was applied to the regression of the reorientation autocorrelation function due to the low signal-to-noise ratio of the correlation function at large time intervals.

$$P_{\mathrm{mKWW}}(t) = \chi e^{-\frac{t}{\tau_0}} + (1-\chi)e^{-\left(\frac{t}{\tau_{\mathrm{KWW}}}\right)^{\beta}} \tag{5}$$

τ_0 and τ_{KWW} are two characteristic times of the mKWW function. The first term, $e^{-\frac{t}{\tau_0}}$, describes the initial exponential decay of the molecule orientation correlations, and $e^{-\left(\frac{t}{\tau_{\mathrm{KWW}}}\right)^{\beta}}$ describes the stretched exponential decay contributions. χ and $(1-\chi)$ are used to weigh the two contributions. β illustrates the width of the stretched exponential decay.

Rotational relaxation time is then calculated through integration of the mKWW function.

$$\begin{aligned}\tau &= \int_0^\infty P_{\mathrm{mKWW}}(t)\mathrm{d}t = \chi\tau_0 + (1-\chi)\tau_{\mathrm{KWW}}\frac{1}{\beta}\Gamma\left(\frac{1}{\beta}\right)\\ &\approx \int_0^\infty C^1(t)\mathrm{d}t.\end{aligned} \tag{6}$$

Here Γ is the gamma function.

Therefore, at low pressures, NEMD calculations should be performed at the targeted temperature of interest because it can directly capture the first Newtonian plateau and obtain the low-shear viscosity values. In order to acquire the high-pressure viscosity data at temperatures of practical interest, where the direct NEMD calculations can hardly capture the first Newtonian plateau, NEMD calculations will be first performed for elevated temperatures and then extrapolated to the temperature of interest using the temperature–viscosity relationship (Eq. 2). At the elevated temperature, the relaxation time should be shorter and therefore the critical shear rate should be higher [32], allowing the capture of the first Newtonian plateau. The magnitude of the required temperature increase is determined based on the calculation of the reciprocal of the rotational relaxation time, which corresponds to the critical shear rate. Figure 3 shows the flow chart for the numerical approach. In order to evaluate the effectiveness of the viscosity extrapolation from the high temperatures, 95 % confidence intervals were calculated for the temperature of interest using the NLPARCI function in MATLAB based on the elevated temperature results. Computational results were then compared with experimental results by Bair [42].

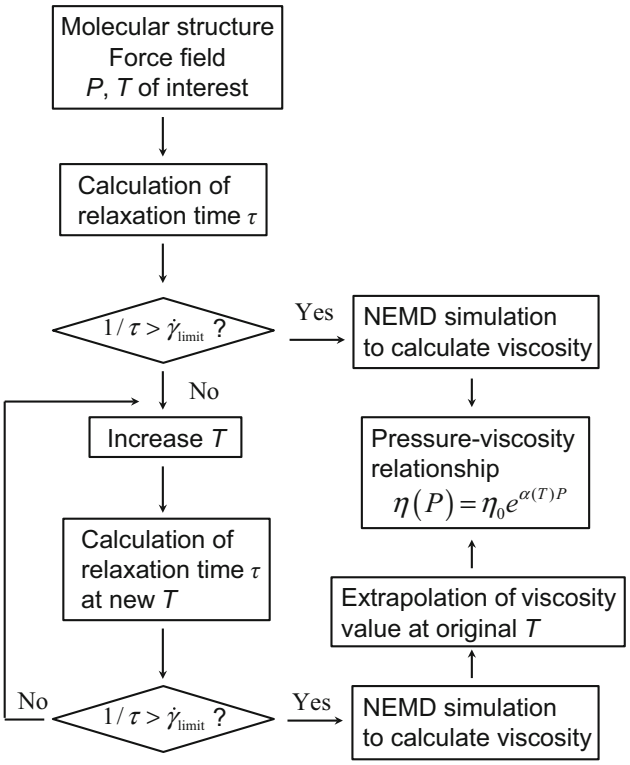

Fig. 3 Flow chart for calculation of the α value of alkanes

3 Simulation Details

The united atom (UA) method was used to generate the 1-Decene trimer. Each of CH_3, CH_2 and CH was considered as a pseudoatom within the hydrocarbon chain with the interaction center at the center of each carbon atom. 100 °C is the temperature of interest in the current study.

The force field used to describe the alkane molecules is similar to the one used by McCabe et al. [32] as its calculated α value of 9-octylheptadecane reached an excellent agreement with experimental measurements though it underestimated the absolute viscosity values in general. This force field was proposed by Siepmann et al. [43] and later extended to branched alkanes by Mondello and Grest [44]. Moreover, the fixed bond length was replaced by a stiff harmonic potential to generate a fully flexible bond [45].

Non-bonded interactions are described with a pairwise Lennard-Jones (LJ) potential [46],

$$V_{\mathrm{LJ}}(r) = 4\varepsilon_{ij}\left[\left(\frac{\sigma_{ij}}{r}\right)^{12} - \left(\frac{\sigma_{ij}}{r}\right)^{6}\right], \tag{7}$$

where ε_{ij} is the depth of the potential well, r is the distance between particles and σ_{ij} is the LJ size. The LJ parameters for interaction between like pseudoatoms are listed in Table 1. Unlike interactions are computed using the standard Lorentz–Berthelot combining rules, shown below.

$$\begin{aligned} \sigma_{ij} &= \frac{\sigma_{ii} + \sigma_{jj}}{2} \\ \varepsilon_{ij} &= \sqrt{\varepsilon_{ii}\varepsilon_{jj}} \end{aligned} \tag{8}$$

The cutoff distance was set at 11.5 Å.

The bond-stretching and bond-bending interactions are described by harmonic potentials, shown below,

$$V_{\mathrm{str}}(l) = \frac{1}{2}k_{\mathrm{str}}\left(l - l_{\mathrm{eq}}\right)^2 \tag{9}$$

$$V_{\mathrm{ben}}(\theta) = \frac{1}{2}k_{\mathrm{ben}}\left(\theta - \theta_{\mathrm{eq}}\right)^2 \tag{10}$$

where k_{str} and k_{ben} are force constants and l_{eq} and θ_{eq} are the equilibrium distance and angle, respectively.

The torsional interaction is described by the model proposed by Jorgensen et al. [47]

$$V_{\mathrm{tor}}(\phi) = \sum_{m=0}^{3} a_m(\cos\phi)^m \tag{11}$$

Table 1 Parameters for the Lennard-Jones potential

Group	ε (Kcal/mol)	σ (Å)
CH_3	0.227	3.93
CH_2	0.093	3.93
CH	0.08	3.81

where a_m are parametric constants. Parameters for intramolecular interactions are given in Table 2.

80 molecules were generated in the system. The system was first created and relaxed in the Materials Studios software to acquire the initial distribution of the pseudoatoms. Then the system runs for 10 nanoseconds to allow the system to reach further equilibrium at the assigned temperature and pressure. This equilibrium configuration provides the initial point for the NEMD simulations. The alkanes then underwent a planar Couette flow using the SLLOD equations of motion [21]. The Lees–Edwards periodic boundary conditions were applied. A Nosé/Hoover thermostat was coupled to achieve energy conservation of the system, as proposed by Tuckerman et al. [48]. The measured resulting shear stress divided by the imposed strain is the value of the shear viscosity. The LAMMPS software [49, 50] was used for the MD simulations, and the timestep of 1 femtosecond was applied in the simulations.

Table 2 Parameters for the intramolecular interactions

	Value	Unit
k_{str}	901.24	Kcal/(mol Å^2)
l_{eq}	1.54	Å
k_{ben}	124.28	Kcal/(mol rad^2)
θ_{eq}	114	Degree
a_0 (X-CH_2-CH_2-Y)	2.007	Kcal/mol
a_1	4.012	Kcal/mol
a_2	0.271	Kcal/mol
a_3	−6.290	Kcal/mol
a_0 (X-CH_2-CH-Y)	0.814	Kcal/mol
a_1	1.792	Kcal/mol
a_2	0.389	Kcal/mol
a_3	−3.673	Kcal/mol

4 Results

Kinematic viscosity and density of the 1-Decene trimer with respect to temperature at pressure of 0.1 MPa are shown in Fig. 4. Based on extrapolation using the temperature viscosity relationship, the kinematic viscosities for 1-Decene trimer at $T = 40$ and 100 °C are 6.7 and 1.53 cSt, respectively, after curve fitting the calculated data. Compared with the experimental data of 16.25 and 3.74 cSt at 40 and 100 °C, respectively, an underprediction of a factor of 2.43–2.44 in absolute value was found, while an accurate prediction of the slope itself. Density values of 0.8 and 0.76 g/cm^3 were used based on the MD calculations of 1-Decene trimer at 0.1 MPa and temperatures of 40 and 100 °C, respectively. Density calculations were compared with a commercially available MSDS data sheet for PAO4cSt [51]. Although PAO 4 also contains certain amount of 1-Decene dimer and tetramer, a rough comparison can be made. Density at 15.6 °C was reported to be 0.82 g/cm^3, comparable to 0.819 g/cm^3 acquired from the current MD simulations. The boiling point was reported to be 687 K, which corresponds well to the range of 673–698 K from the current MD simulations, where a significant change in density was observed.

The relaxation times were calculated for various pressures at 100 °C to determine a suitable pressure at which the switch from the direct NEMD to NEMD committed at elevated temperatures. Figure 5 shows the mKWW function fit of the calculated autocorrelation function for 400 MPa, and the relaxation time was determined to be 5.2 ns. As mentioned before, the signal-to-noise ratio of the autocorrelation function deteriorates for large time intervals, and the parameters were adjusted to best fit the initial portion of the curve; 400 MPa was taken as a suitable division of the direct NEMD and NEMD approaches at elevated temperatures as the critical shear rate is estimated at around 2×10^8 s^{-1}, which is slightly larger than the minimum applicable NEMD shear limit to ensure the capture of the first Newtonian plateau.

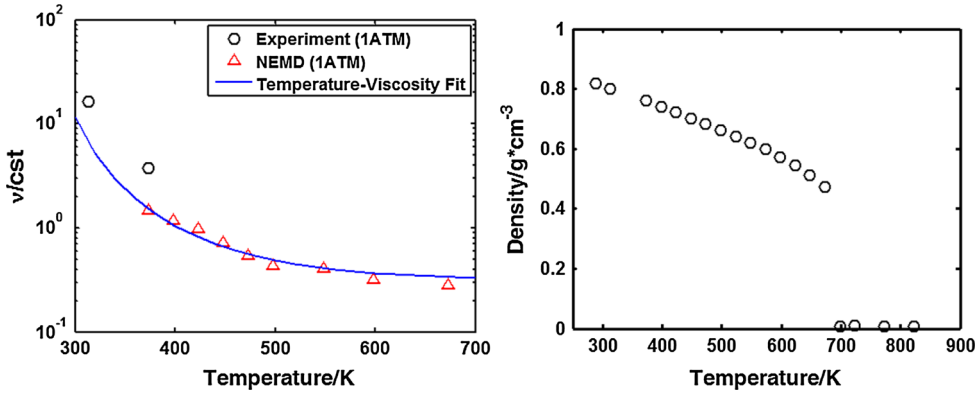

Fig. 4 Kinematic viscosity and density versus temperature at 0.1 MPa pressure, respectively

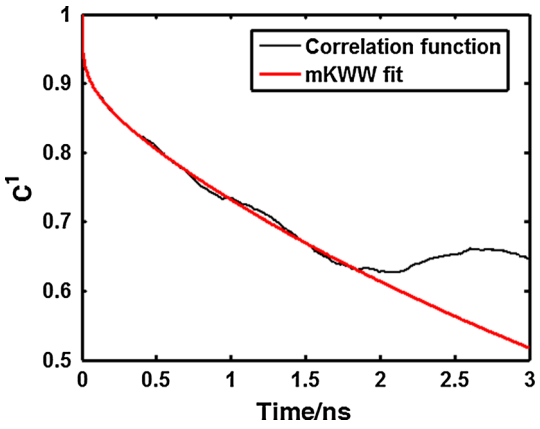

Fig. 5 mKWW fit of the reorientation autocorrelation function of the longest principal axis of the molecule ellipsoid of inertia for 400 MPa, 100 °C

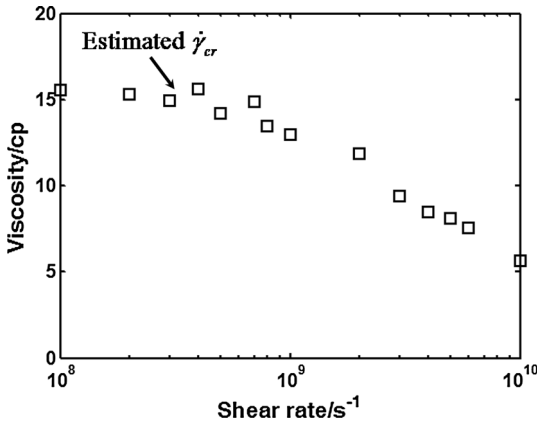

Fig. 7 Calculated viscosities at different shear rates under 600 MPa, 175 °C. The arrow points the estimated critical shear rate calculated from the reciprocal of the rotational relaxation time

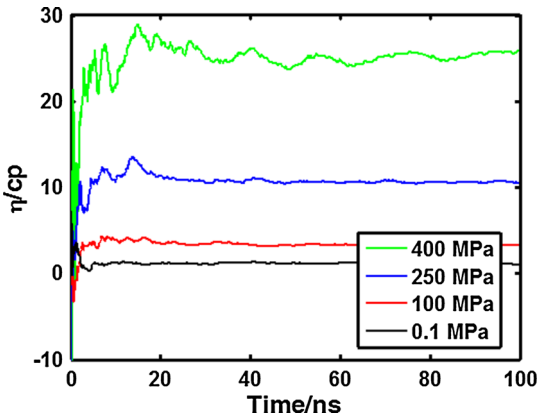

Fig. 6 Calculated viscosity values with respect to increasing calculation time

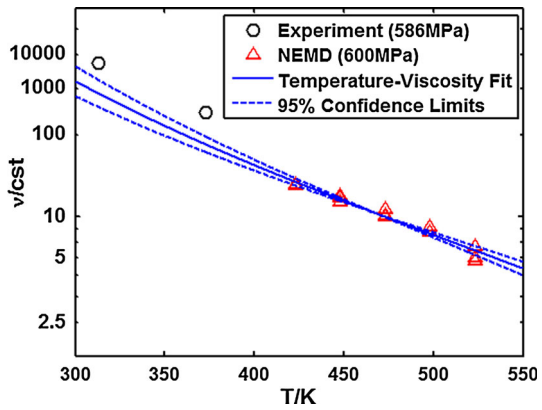

Fig. 8 Viscosities calculated and extrapolated for 600 MPa

Figure 6 shows the viscosity results with respect to the total calculation time of various pressure at $T = 100$ °C. The shear rate of 2×10^8 s^{-1} was applied to the pressures of 0.1, 100, 250 MPa, and the shear rate of 10^8 s^{-1} was applied to the pressure of 400 MPa, respectively. As computation time increases, viscosity gradually reaches a constant value though data oscillation could still be observed. For the cases with a larger rotational relaxation time (or a higher pressure), convergence is more difficult to reach. Based on the observed oscillation of viscosity data, total calculation of about 5–20 times the rotational relaxation time is recommended to reach equilibrium, and this in turn would result in 50–200 ns if the critical shear rate is at the NEMD limit of 10^8 s^{-1}. The total NEMD calculation time of 100 ns for each data point is therefore believed to be a suitable time period, and is used for further calculations. However, non-convergent solutions were still observed for certain cases, and this may be due to certain configuration at the starting point of the NEMD simulations.

The shear viscosities at 600 MPa and 175 °C of different shear rates were calculated and are shown in Fig. 7. The critical shear rate was found to be 3.07×10^8 s^{-1} from the calculations of the reciprocal of the rotational relaxation time, as marked by the arrow, which agreed well with the calculated NEMD results to show the onset of the shear thinning behavior. At high strain rates, the system showed a shear thinning behavior, while the viscosity results at different shear rates lower than the critical shear rate were consistent, suggesting that the current approach indeed captured the first Newtonian plateau of the lubricant. Therefore, it is valid to take calculated viscosities at shear rates below the critical shear rate as the low-shear viscosity values at the targeted temperature and pressure.

Figures 8, 9 and 10 show the extrapolation of viscosities to lower temperature for high pressures of 600 MPa, 800 MPa and 1 GPa. Constant c in Eq. 2 is taken as 0.7 in the current analyses. For higher pressures, a larger increase

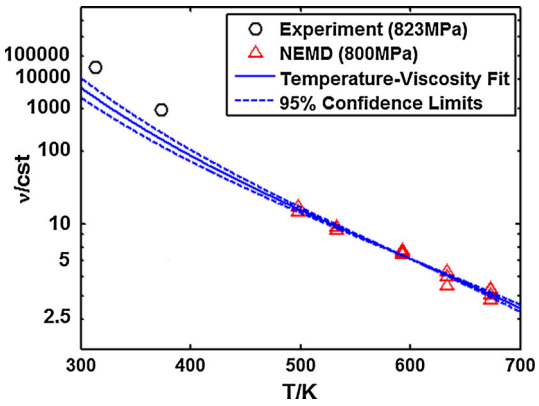

Fig. 9 Viscosities calculated and extrapolated for 800 MPa

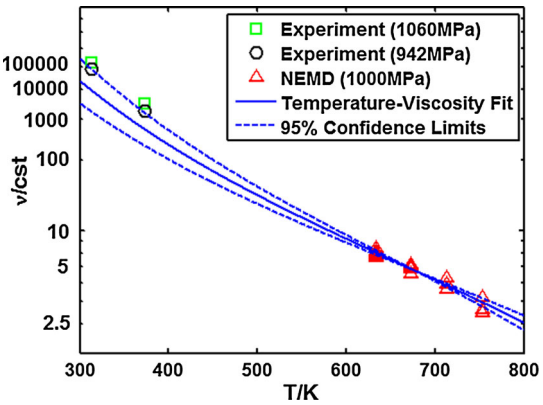

Fig. 10 Viscosities calculated and extrapolated for 1 GPa

in temperature is needed to capture the first Newtonian plateau with the NEMD calculations. Meanwhile, for higher temperatures, the applicable NEMD shear rate limit further increases as the signal-to-noise ratio further deteriorates. This in turn requires significant temperature increase for the pressure of 1 GPa, compared to that for the 600 or 800 MPa case. Different initial configurations were used for each individual calculation. Different shear rates that were less than the critical shear rate were used for each case to further validate the capture of the first Newtonian plateau. The values were first shown on the semilog plot and then rescaled to the double-log plot. For all three cases, the absolute viscosity values were lower than the experimental data as expected; however, they demonstrated a good trend even till the low temperature of 40 °C. 95 % confidence limits were calculated based on the available data points to ensure the effectiveness of extrapolations. The author also examined extrapolations using the VFTH equation (Eq. 3); however, due to the nonlinear nature of this equation, the 95 % confidence limit would suggest a value range of two or three magnitudes, diminishing the usefulness of the extrapolation.

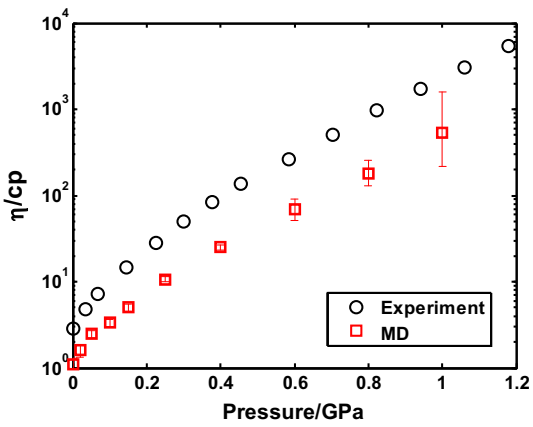

Fig. 11 Semilog plot of the viscosity as a function of pressure for 1-Decene trimer. Note that the trend shows a systematic difference between the two curves, but their slopes are similar

Table 3 Comparisons of α_0 and α^* from experimental data and MD data

	Experiments [42]	MD	Relative error (%)
α_0	16.3	16.5	1.2
α^*	10.9	10.1	7.3

Figure 11 compares the experimental results [42] and MD calculations of the pressure–viscosity relationship. The error bars for the first seven data points (from direct NEMD) were smaller than the marker size. The error bar values for the last three data points (from extrapolations of the NEMD calculations with elevated temperatures) were taken from the upper and lower limits of the 95 % confidence intervals. As expected, the variation increased with pressure due to extrapolations from higher temperatures. Variation of the viscosity values extrapolated from 1 GPa is significantly larger than that from the 600 and 800 MPa cases, suggesting that the calculations for even higher pressure is less recommended. While the absolute variation at each temperature was found to be about the same, percentage wise this would suggest a larger variation for higher temperature cases. For higher pressure cases, more data points are required to obtain a trustable confidence level. Comparison between the calculated α_0 and α^* with the experimental data [42] is shown in Table 3. It should be mentioned the impurity of the samples used in the experiments may also contribute to the difference. Nevertheless, the α values demonstrated a good agreement between the measurements and the NEMD calculations. Densities of the 1-Decene trimer for 600 MPa, 800 MPa and 1 GPa at 100 °C taken from the MD calculation are 0.965, 0.996 and 1.021 g/cm^3, respectively. Figure 12 shows the viscosity comparison after dividing the viscosity value at 0.1 MPa

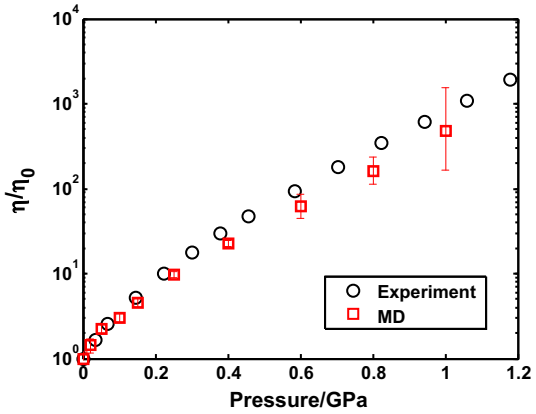

Fig. 12 Relative viscosity after normalization with viscosity value at 0.1 MPa

(η_0) of the two curves to shift the curves so that they share the same initial value at 0.1 MPa. It reveals that the MD simulations can capture the viscosity change with pressure accurately while underpredict the absolute viscosity value. The difference gradually increases with temperature, which contributed to the slight underestimation of α^*. Such discrepancy may also be due to the inaccuracy of the Walther equation at such a large temperature and pressure range, because its extrapolations at high and low temperatures have both shown noticeable errors [52]. A more accurate empirical temperature–viscosity relationship available for a wide temperature range should be more helpful.

5 Conclusions

Viscosity calculations for a branched alkane under various pressures and temperatures were achieved through direct NEMD together with a TTS-based extrapolations from NEMD at elevated temperatures based on the analyses of the rotational relaxation time. The data were used to obtain the pressure–viscosity coefficient, α_0 and α^*, of this typical base oil. The calculated α values agree well with experimentally measured data, although the absolute values of the shear viscosity were underestimated in general. Relative comparison of the experimental and calculated pressure–viscosity curves suggests a promising method for evaluating pressure–viscosity relationships of base oils in the range of C_{20}–C_{40}. Acquisition of a more accurate and convenient temperature–viscosity model of a linear nature for extrapolation would further help improve the accuracy of the α^* prediction.

Acknowledgments The authors would like to express sincere gratitude to the financial support from Ashland Inc. This research was also supported in part through the computational resources and staff contributions provided for the Quest high performance computing facility at Northwestern University which is jointly supported by the Office of the Provost, the Office for Research, and Northwestern University Information Technology.

References

1. Bair, S., Liu, Y., Wang, Q.J.: The pressure–viscosity coefficient for Newtonian EHL film thickness with general piezoviscous response. J. Tribol. **128**(3), 624–631 (2006)
2. Bair, S., Qureshi, F.: Accurate measurements of pressure–viscosity behavior in lubricants. Tribol. Trans. **45**(3), 390–396 (2002)
3. Seeton, C.: Viscosity–temperature correlation for liquids. Tribol. Lett. **22**(1), 67–78 (2006)
4. Totten, G.E., Westbrook, S.R., Shah, R.J.: Fuels and Lubricants Handbook: Technology, Properties, Performance, and Testing, vol. 37. ASTM International, Pennsylvania (2003)
5. Vogel, H.: Das temperaturabhängigkeitsgesetz der viskosität von flüssigkeiten. Phys. Z **22**, 645–646 (1921)
6. Fulcher, G.S.: Analysis of recent measurements of the viscosity of glasses. J. Am. Ceram. Soc. **8**(6), 339–355 (1925)
7. Tammann, G., Hesse, W.: Die Abhängigkeit der Viscosität von der Temperatur bie unterkühlten Flüssigkeiten. Zeitschrift für anorganische und allgemeine Chemie **156**(1), 245–257 (1926)
8. Stachowiak, G., Batchelor, A.W.: Engineering Tribology. Butterworth-Heinemann, Oxford (2013)
9. Schaschke, C.J.: High pressure viscosity measurement with falling body type viscometers. Int. Rev. Chem. Eng. **2**(5), 564–576 (2010)
10. Bair, S.: A routine high-pressure viscometer for accurate measurements to 1 GPa. Tribol. Trans. **47**(3), 356–360 (2004)
11. Cook, R.L., Herbst, C.A., King Jr, H.: High-pressure viscosity of glass-forming liquids measured by the centrifugal force diamond anvil cell viscometer. J. Phys. Chem. **97**(10), 2355–2361 (1993)
12. Hamrock, B.J., Dowson, D.: Isothermal elastohydrodynamic lubrication of point contacts: part III—fully flooded results. J. Lubr. Technol. **99**(2), 264–275 (1977)
13. Hamrock, B.J., Dowson, D.: Isothermal elastohydrodynamic lubrication of point contacts: Part 1—theoretical formulation. J. Lubr. Technol. **98**(2), 223–228 (1976)
14. Ramasamy, U.S., Bair, S., Martini, A.: Predicting pressure–viscosity behavior from ambient viscosity and compressibility: challenges and opportunities. Tribol. Lett. **57**(2), 1–7 (2015)
15. Wu, C., Klaus, E., Duda, J.: Development of a method for the prediction of pressure–viscosity coefficients of lubricating oils based on free-volume theory. J. Tribol. **111**(1), 121–128 (1989)
16. Mondello, M., Grest, G.S.: Molecular dynamics of linear and branched alkanes. J. Chem. Phys. **103**(16), 7156–7165 (1995)
17. Nath, S.K., Escobedo, F.A., de Pablo, J.J.: On the simulation of vapor–liquid equilibria for alkanes. J. Chem. Phys. **108**, 9905 (1998)
18. Martin, M.G., Siepmann, J.I.: Novel configurational-bias Monte Carlo method for branched molecules. Transferable potentials for phase equilibria. 2. United-atom description of branched alkanes. J. Phys. Chem. B **103**(21), 4508–4517 (1999)
19. Padilla, P., Toxværd, S.: Self-diffusion in *n*-alkane fluid models. J. Chem. Phys. **94**(8), 5650–5654 (1991)
20. Chang, J., Sandler, S.I.: Interatomic Lennard-Jones potentials of linear and branched alkanes calibrated by Gibbs ensemble simulations for vapor–liquid equilibria. J. Chem. Phys. **121**(15), 7474–7483 (2004)
21. Evans, D., Morriss, G.: Statistical Mechanics of Nonequilibrium Liquids. Cambridge University Press, Cambridge (2008)

22. Morriss, G.P., Daivis, P.J., Evans, D.J.: The rheology of n alkanes: Decane and eicosane. J. Chem. Phys. **94**(11), 7420–7433 (1991)
23. Cui, S., Cummings, P., Cochran, H., Moore, J., Gupta, S.: Nonequilibrium molecular dynamics simulation of the rheology of linear and branched alkanes. Int. J. Thermophys. **19**(2), 449–459 (1998)
24. Cui, S., Gupta, S., Cummings, P., Cochran, H.: Molecular dynamics simulations of the rheology of normal decane, hexadecane, and tetracosane. J. Chem. Phys. **105**(3), 1214–1220 (1996)
25. Khare, R., de Pablo, J., Yethiraj, A.: Rheological, thermodynamic, and structural studies of linear and branched alkanes under shear. J. Chem. Phys. **107**, 6956 (1997)
26. Kioupis, L.I., Maginn, E.J.: Molecular simulation of poly-α-olefin synthetic lubricants: impact of molecular architecture on performance properties. J. Phys. Chem. B **103**(49), 10781–10790 (1999)
27. Moore, J., Cui, S., Cochran, H., Cummings, P.: Rheology of lubricant basestocks: a molecular dynamics study of C_{30} isomers. J. Chem. Phys. **113**(19), 8833–8840 (2000)
28. Jabbarzadeh, A., Atkinson, J., Tanner, R.: Effect of molecular shape on rheological properties in molecular dynamics simulation of star, H, comb, and linear polymer melts. Macromolecules **36**(13), 5020–5031 (2003)
29. Moore, J., Cui, S., Cummings, P., Cochran, H.: Lubricant characterization by molecular simulation. AIChE J. **43**(12), 3260–3263 (1997)
30. Mundy, C.J., Klein, M.L., Siepmann, J.I.: Determination of the pressure–viscosity coefficient of decane by molecular simulation. J. Phys. Chem. **100**(42), 16779–16781 (1996)
31. Kioupis, L.I., Maginn, E.J.: Impact of molecular architecture on the high-pressure rheology of hydrocarbon fluids. J. Phys. Chem. B **104**(32), 7774–7783 (2000)
32. McCabe, C., Cui, S., Cummings, P.T., Gordon, P.A., Saeger, R.B.: Examining the rheology of 9-octylheptadecane to gigapascal pressures. J. Chem. Phys. **114**, 1887 (2001)
33. Bair, S., Qureshi, F.: The generalized Newtonian fluid model and elastohydrodynamic film thickness. J. Tribol. **125**(1), 70–75 (2003)
34. Gordon, P.A.: Development of intermolecular potentials for predicting transport properties of hydrocarbons. J. Chem. Phys. **125**, 014504 (2006)
35. Gordon, P.A.: Characterizing isoparaffin transport properties with Stokes–Einstein relationships. Ind. Eng. Chem. Res. **42**(26), 7025–7036 (2003)
36. Pan, G., McCabe, C.: Prediction of viscosity for molecular fluids at experimentally accessible shear rates using the transient time correlation function formalism. J. Chem. Phys. **125**, 194527 (2006)
37. Morriss, G.P., Evans, D.J.: Application of transient correlation functions to shear flow far from equilibrium. Phys. Rev. A **35**(2), 792 (1987)
38. Evans, D.J., Morriss, G.P.: Transient–time-correlation functions and the rheology of fluids. Phys. Rev. A **38**(8), 4142 (1988)
39. Bair, S., McCabe, C., Cummings, P.T.: Comparison of nonequilibrium molecular dynamics with experimental measurements in the nonlinear shear-thinning regime. Phys. Rev. Lett. **88**(5), 58302 (2002)
40. Hansen, J.-P., McDonald, I.R.: Theory of simple liquids. Elsevier, Amsterdam (1990)
41. Williams, G., Watts, D.C.: Non-symmetrical dielectric relaxation behaviour arising from a simple empirical decay function. Trans. Faraday Soc. **66**, 80–85 (1970)
42. Bair, S.: The high pressure rheology of some simple model hydrocarbons. Proc. Inst. Mech. Eng., J: J. Eng. Tribol. **216**(3), 139–149 (2002)
43. Siepmann, J.I., Karaborni, S., Smit, B.: Simulating the critical behaviour of complex fluids. Nature **365**, 330–332 (1993)
44. Mondello, M., Grest, G.S.: Molecular dynamics of linear and branched alkanes. J. Chem. Phys. **103**(16), 7156 (1995)
45. Mundy, C.J., Siepmann, J.I., Klein, M.L.: Calculation of the shear viscosity of decane using a reversible multiple time-step algorithm. J. Chem. Phys. **102**(8), 3376 (1995)
46. Lennard-Jones, J.E.: Cohesion. Proc. Phys. Soc. **43**(5), 461 (1931)
47. Jorgensen, W.L., Madura, J.D., Swenson, C.J.: Optimized intermolecular potential functions for liquid hydrocarbons. J. Am. Chem. Soc. **106**(22), 6638–6646 (1984)
48. Tuckerman, M.E., Mundy, C.J., Balasubramanian, S., Klein, M.L.: Modified nonequilibrium molecular dynamics for fluid flows with energy conservation. J. Chem. Phys. **106**(13), 5615–5621 (1997)
49. Plimpton, S.: Fast parallel algorithms for short-range molecular dynamics. J. Comput. Phys. **117**(1), 1–19 (1995)
50. LAMMPS WWW Site. http://lammps.sandia.gov
51. Material Safety Data Sheet for PAO 4 cSt. http://www.cpchem.com/msds/100000010950_SDS_JP_EN.PDF
52. Booser, E.R.: CRC handbook of lubrication. Theory and practice of tribology: volume II: theory and design. CRC Press Inc., Florida (1984)